

Measurements of surface-wave damping in a container

David R. Howell

School of Physics, Georgia Institute of Technology, Atlanta, Georgia 30332

Ben Buhrow

Department of Physics, University of Northern Iowa, Cedar Falls, Iowa 50614

Ted Heath and Conor McKenna

School of Physics, Georgia Institute of Technology, Atlanta, Georgia 30332

Wook Hwang

California Institute of Technology, Pasadena, California 91125

Michael F. Schatz^{a)}

School of Physics, Georgia Institute of Technology, Atlanta, Georgia 30332

(Received 14 October 1998; accepted 20 October 1999)

For surface waves in brimful right circular cylinders with clean interfaces and pinned contact lines, damping rates and frequencies are measured for the six lowest frequency surface-wave modes over a two-decade range of the inverse Reynolds number C . Asymptotic calculations that include viscous dissipation in both Stokes boundary layers and the bulk show good agreement with measurements for small C ; the theory typically overpredicts the measured damping rates for C large. Our measurements suggest interfacial contamination may account for a previously reported discrepancy between theory and experiment. © 2000 American Institute of Physics. [S1070-6631(00)00702-9]

I. INTRODUCTION

The decay rate for surface waves in a container has proven to be surprisingly difficult to predict quantitatively. Some damping mechanisms are inherently complex: Examples include damping by free surface contamination (a consequence of “pouring oil on troubled waters,” as noted by Aristotle, Plutarch, and Pliny the Elder¹) and by contact line motion at the lateral boundary.² Nevertheless, even in the case where contamination and moving contact lines are absent, theoretical predictions, which often only include damping due to (oscillatory) Stokes boundary layers near the bottom and sides of the container, can underestimate measured damping rates by as much as a factor of 4.^{3,4}

Recent calculations by Martel *et al.*⁵ suggest predictions may be improved dramatically by including the effects of viscous dissipation in the bulk of the liquid layer. For a brimful right circular container with a clean surface and a pinned contact line, Martel *et al.* find damping rates that agree to within 4% for five out of six modes measured in the experiments of Henderson and Miles (henceforth referred to as HM,³); for the sixth mode, theory underpredicts experiment by 26%. Later calculations^{6,7} yield essentially the same result, leaving this discrepancy unresolved. With the availability of only these six data points (at a single fixed set of parameter values) for comparison, the degree to which the inclusion of bulk damping improves predictions for a broad range of experimental conditions has, heretofore, remained untested.

We report measurements of modal damping rates and

frequencies in experiments that achieve a two-decade variation in the inverse Reynolds number C (Fig. 1), which characterizes the damping. To make connection with earlier experiments, we study modes in one container that is nearly identical in geometry and construction to that used in HM; a second container of substantially different aspect ratio Γ is also investigated. Developing an experimentally proven approach for predicting linear damping is an important step toward building a fully self-consistent weakly nonlinear theory for the evolution of waves in many fundamental and practical problems involving confined liquids with free surfaces; examples include pattern formation and transport in Faraday waves^{8,9} and oscillations in liquid bridges, a hydrodynamic model for float-zone refining.¹⁰

II. BACKGROUND

Experiments are conducted with right cylindrical containers filled to the brim with fluids whose kinematic viscosities ν range over two orders of magnitude. An acrylic container that closely follows the design used by HM is constructed with depth $d = 2.764 \pm 0.005$ cm and aspect ratio $\Gamma = 0.725$. A second container, which has $d = 1.180 \pm 0.005$ cm and $\Gamma = 4.33$, is fabricated with an aluminum sidewall and acrylic bottom. Both silicone oils (polydimethylsiloxanes—Dow Corning 200® Fluids) and highly purified water (High Performance Liquid Chromatography (HPLC) grade, Sigma-Aldrich, Inc.) are used in the $\Gamma = 0.725$ container; only silicone oils are investigated in the $\Gamma = 4.33$ container. The rim of each container is sharpened on the inner diameter to provide a uniform, well-defined edge to pin the contact line. For the silicone oils, the rim is coated with a fluoropolymer (FluoroPel™ PFC1601A, Cy-

^{a)}Electronic mail: mike.schatz@physics.gatech.edu

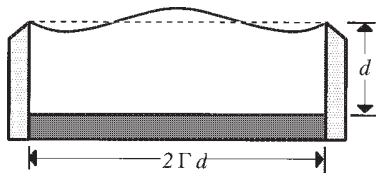


FIG. 1. Surface-wave damping is investigated in clean liquid layers with a contact line pinned to a circular lateral boundary, as shown in a schematic cross section of the experiment. The experimental conditions are described by the aspect ratio Γ , the inverse Reynolds number $C \equiv (\nu/\sqrt{g(d\Gamma)^3})$ and the Bond number $B \equiv g\rho(d\Gamma)^2/\sigma$ with the liquid's depth d , density ρ , surface tension σ , kinematic viscosity ν and the earth's gravitational acceleration g .

tonix Corp.) to ensure a partially wetting, equilibrium condition for the static contact line at the edge; the container rim is uncoated for HPLC water. The flatness of the liquid surface is determined by observing the reflection of a straight edge; the surface is flat when the reflection is undistorted near the contact line. This method yields layers of reproducible depth, as confirmed by independent measurement with a mechanical gauge. During the runs, the temperature of the fluid is monitored continually and measured to an accuracy of 0.1 °C. At the operating temperatures of the silicone oils, ν is measured with Cannon–Fenske Routine viscometers (Cannon Instrument Co.), surface tension σ is measured using digital imaging of pendant drops,¹¹ and density ρ is measured using a specific gravity cup (Table I). For water, ν , σ , and ρ are obtained from published data.¹² The governing nondimensional parameters C , Γ , and the Bond number B (Fig. 1) are fully determined by specifying these properties in conjunction with the container geometry.

Vertical vibration of the container parametrically excites surface wave modes (Faraday modes), which are characterized by ordered pairs (mq) where m is the number of radial nodes and q is the number of azimuthal nodes (excluding the node enforced by the pinned contact line). The container is mounted on an inductively driven linear translation stage (linear motor), which is vertically vibrated at approximately twice the natural frequency of the mode under study. The motor is driven by a bipolar power supply, which, in turn, is under open-loop computer control via a 12-bit analog voltage output. Under these conditions, the container motion is sinusoidal, as verified by measurements in separate experi-

TABLE I. Kinematic viscosity ν surface tension σ and density ρ for working fluids in the experiments. The last row entry corresponds to experiments with high purity water; all other row entries correspond to experiments with silicone oils.

Viscosity (cm ² /s)	Surface Tension σ (dyne/cm)	Density ρ (g/cm ³)
1.10×10^{-2}	16.35	0.818
2.22×10^{-2}	17.32	0.873
5.50×10^{-2}	18.20	0.914
1.11×10^{-1}	19.08	0.935
2.52×10^{-1}	19.51	0.947
5.33×10^{-1}	20.06	0.963
1.07	20.28	0.969
9.04×10^{-3}	72.40	0.998

ments using a capacitive displacement transducer. For a properly chosen excitation amplitude, the filled container is vibrated for 30–120 s before the initially flat oil–air interface becomes unstable to waves; when the waves reach a steady-state saturation amplitude where both m and q can be easily verified visually, the vertical excitation is turned off and the waves decay.

The amplitude of decaying waves is typically monitored nonintrusively by tracking the reflection of a red diode laser beam from the liquid–air interface. The incident beam is normal to the initially flat interface. As a result, the reflected beam is unaffected by changes in the liquid depth and is deflected solely by changes in slope at the interface. A beam-splitter directs the reflected beam to strike the surface of a position sensing detector (Model 1L30, On-Trak Photonics, Inc.), which tracks the average position of the intercepted beam. When the interface is undisturbed, the intercepted beam is normally incident on the center of the detector; when the interface is in motion, the detector subtends the angle through which the beam moves, permitting real-time measurement of the interface slope. In some experiments, we also measured the height of surface waves using a noncontact capacitive probe (Model TPC-200, Capacitec, Inc.), in a manner similar to that employed by HM. Both methods often yield the same result. However, we find that for the highest frequency modes in the $\Gamma = 0.725$ container, damping rates measured using the capacitive probe depend somewhat on the lateral positioning of the probe; we attribute this variation to the coupling of the probe's nonuniform electric field to the laterally varying interface shape over the ~ 0.8 cm diam region interrogated by the probe. No such spatial dependence is found with the laser probe, which senses a much smaller lateral region (~ 0.1 cm diam), and, therefore, yields measurements that are less sensitive to the undesired effects of spatial averaging.

Complex demodulation¹³ of the surface-slope time series yields the measured damping rates δ_e and frequencies ω_e (Fig. 2). A time interval is selected where the surface slope has small amplitude and decays symmetrically about the mean position of the interface [e.g., 10 s $< t <$ 45 s in Fig. 2(a)]. The time series is repeatedly complex-demodulated with iterative changes in the modulation frequency. The frequency ω_e of the surface-wave mode is equal to the modulation frequency that minimizes the phase change for the time interval of interest [Fig. 2(b)]. A semilog plot of complex-demodulated amplitude exhibits a linear behavior over this same time interval [Fig. 2(c)]; the slope of a line fitted to the data yields the decay rate δ_e for the surface waves.

Predicted damping rates δ_l and frequencies ω_l are computed using the asymptotic calculation method developed by Martel *et al.*⁵ In brief, normal mode solutions (described by the velocity, pressure, and surface deformation fields as well as the damping rate and frequency) are expanded in powers of $C^{1/2}$ to order C in the linearized governing equations and boundary conditions. An integral solvability condition⁵ is used to overcome the difficulty that a contact line singularity, which becomes stronger with increasing powers of C , often causes perturbation calculations to fail at $O(C)$.¹⁴ Solution

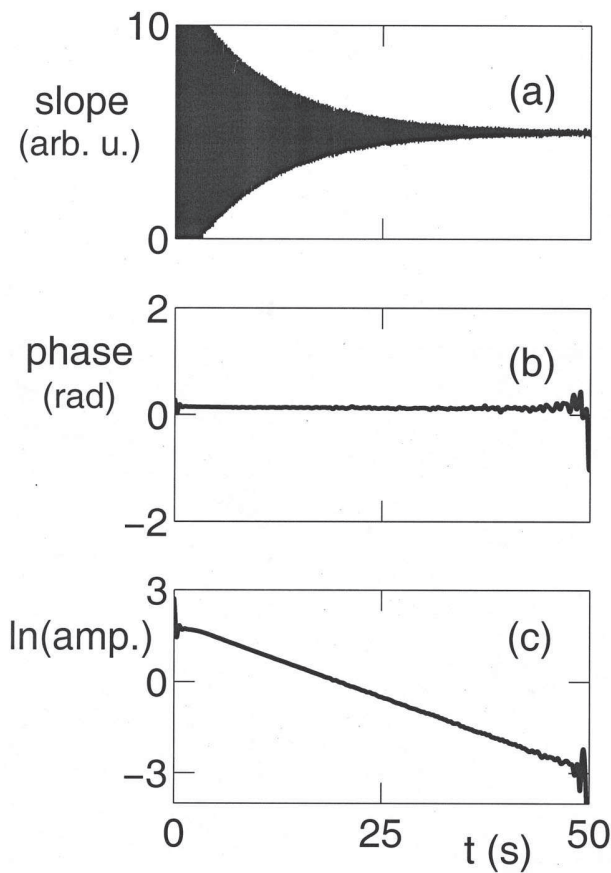


FIG. 2. Measured surface-slope time series (a), with complex-demodulated phase (b), and amplitude (c), for a (0,1) mode in silicone oil with $C = 7.647 \times 10^{-5}$ and $\Gamma = 0.725$.

of the resulting boundary-value problem leads to predicted damping rates and frequencies of the form

$$\delta_t = a_1 C^{1/2} + a_2 C, \quad \omega_t = a_0 - a_1 C^{1/2}, \quad (1)$$

where a_0 is obtained from $O(1)$ inviscid solution, $a_1 C^{1/2}$ describes the first approximation to viscous dissipation in the Stokes layers, and $a_2 C$ includes the effects of both viscous dissipation in the bulk and a higher order correction to the damping in the Stokes layers. (At the next highest order for both ω_t and δ_t [$O(C^{3/2})$], the first contribution from damping in the free surface boundary layer arises; this effect as well as all other terms beyond $O(C)$ are neglected.) The computation of a_0 , a_1 , and a_2 as a function of C , B , and Γ corresponding to our experiments follows identically the method of computing the corresponding quantities in Eq. (3.1) of Ref. 5, to which we refer the interested reader for further details.

III. RESULTS

The frequencies ω_t and ω_e typically agree to better than 1% for the 74 separate conditions investigated in our experiments (Tables II–IV). ω_e is weakly dependent on C ; for example, ω_e for the (20) mode decreases by 6.6% when C increases by a factor of 100 for $\Gamma = 4.33$. This characteristic is captured by ω_t [Eq. (1)] since the inviscid term a_0 domi-

TABLE II. Comparison of predictions (ω_t , δ_t) with measurements (ω_e , δ_e) for experiments using HPLC-grade water in a container with $\Gamma = 0.725$ and $B = 103.2$. The ratio $a_1 C^{1/2} / \delta_e$ indicates the relative importance of boundary layer damping for describing the measurements.

C	Mode	ω_e	ω_t / ω_e	δ_e	δ_t / δ_e	$a_1 C^{1/2} / \delta_e$
6.354×10^{-5}	(10)	1.547	1.007	4.620×10^{-3}	1.046	0.852
6.215×10^{-5}	(20)	2.102	1.007	7.231×10^{-3}	0.984	0.693
6.215×10^{-5}	(01)	2.272	1.007	4.380×10^{-3}	0.879	0.336
6.354×10^{-5}	(30)	2.591	1.008	9.774×10^{-3}	0.990	0.598

nates with the viscous term $a_1 C^{1/2}$ accounting for a relatively small correction, even for C large; $(a_1 C^{1/2}) / a_0 = 0.073$ for the (20) mode with $C = 2.96 \times 10^{-3}$ and $\Gamma = 4.33$. [The $O(C)$ term for ω_t is identically zero.⁵] The differences between ω_e and ω_t slightly exceed 1% for some modes at the largest values of C where measurement of frequencies is the most difficult since only a few complete oscillations (in some cases, three at most) are observable before the mode completely decays.

To make direct connection to the experiments of HM,³ damping rates are measured for $C < 10^{-4}$ for $\Gamma = 0.725$ using

TABLE III. Comparison of predictions (ω_t , δ_t) with measurements (ω_e , δ_e) in experiments using silicone oils in a container with $\Gamma = 0.725$. The measurements are effectively carried out at fixed B , despite differences in physical properties as ν changes for the silicone oils, (Table I); the small variation of B in the range $357 \leq B \leq 374$ has a negligible effect on the predictions over this range of C .

C	Mode	ω_e	ω_t / ω_e	δ_e	δ_t / δ_e	$a_1 C^{1/2} / \delta_e$
7.647×10^{-5}	(10)	1.438	1.006	6.017×10^{-3}	0.963	0.796
7.647×10^{-5}	(20)	1.899	1.006	9.030×10^{-3}	0.973	0.708
7.647×10^{-5}	(01)	2.079	1.004	5.157×10^{-3}	0.948	0.389
7.647×10^{-5}	(30)	2.272	1.006	1.173×10^{-2}	0.996	0.635
7.647×10^{-5}	(11)	2.501	1.005	8.203×10^{-3}	0.948	0.301
7.647×10^{-5}	(40)	2.609	1.006	1.553×10^{-2}	0.946	0.527
1.557×10^{-4}	(10)	1.433	1.007	9.080×10^{-3}	0.977	0.755
1.557×10^{-4}	(20)	1.894	1.006	1.401×10^{-2}	0.998	0.653
1.557×10^{-4}	(01)	2.075	1.005	8.815×10^{-3}	0.984	0.325
1.550×10^{-4}	(30)	2.268	1.005	1.962×10^{-2}	0.976	0.542
1.543×10^{-4}	(11)	2.498	1.005	1.458×10^{-2}	0.972	0.241
1.543×10^{-4}	(40)	2.604	1.006	2.515×10^{-2}	0.984	0.464
3.830×10^{-4}	(10)	1.430	1.009	1.553×10^{-2}	1.013	0.692
3.830×10^{-4}	(20)	1.889	1.009	2.539×10^{-2}	1.035	0.564
3.816×10^{-4}	(01)	2.075	1.005	1.808×10^{-2}	1.040	0.248
3.816×10^{-4}	(30)	2.262	1.008	3.715×10^{-2}	1.017	0.449
3.816×10^{-4}	(11)	2.495	1.008	3.033×10^{-2}	1.052	0.182
3.816×10^{-4}	(40)	2.596	1.010	5.010×10^{-2}	1.012	0.366
7.633×10^{-4}	(10)	1.425	1.009	2.427×10^{-2}	1.031	0.624
7.619×10^{-4}	(20)	1.883	1.008	4.262×10^{-2}	1.029	0.473
7.591×10^{-4}	(01)	2.072	1.006	3.321×10^{-2}	1.046	0.189
7.570×10^{-4}	(30)	2.252	1.009	6.294×10^{-2}	1.038	0.372
7.584×10^{-4}	(11)	2.493	1.007	5.566×10^{-2}	1.081	0.140
7.556×10^{-4}	(40)	2.587	1.009	8.804×10^{-2}	1.028	0.292
1.731×10^{-3}	(10)	1.416	1.009	4.201×10^{-2}	1.088	0.542
1.731×10^{-3}	(20)	1.870	1.010	7.513×10^{-2}	1.132	0.404
1.738×10^{-3}	(01)	2.066	1.008	6.596×10^{-2}	1.135	0.144
1.759×10^{-3}	(30)	2.234	1.012	1.166×10^{-1}	1.130	0.305
1.752×10^{-3}	(11)	2.483	1.010	1.170×10^{-1}	1.130	0.101
3.670×10^{-3}	(10)	1.405	1.011	6.804×10^{-2}	1.197	0.487
3.684×10^{-3}	(20)	1.852	1.013	1.364×10^{-1}	1.169	0.324
3.705×10^{-3}	(01)	2.059	1.010	1.272×10^{-1}	1.193	0.109

TABLE IV. Comparison of predictions (ω_i , δ_i) with measurements (ω_e , δ_e) for experiments using silicone oils in a container with $\Gamma=4.33$. The measurements are effectively carried out at fixed B , despite differences in physical properties as ν changes for the silicone oils, (Table I), since the small variation of B in the range $1223 \leq B \leq 1280$ has a negligible effect on the predictions over this range of C .

C	Mode	ω_e	ω_i/ω_e	δ_e	δ_i/δ_e	$a_1 C^{1/2}/\delta_e$
3.047×10^{-5}	(10)	0.884	1.003	9.402×10^{-3}	0.969	0.918
3.047×10^{-5}	(20)	1.413	1.007	1.191×10^{-2}	0.978	0.892
3.047×10^{-5}	(01)	1.688	1.005	8.802×10^{-3}	0.954	0.817
3.047×10^{-5}	(30)	1.862	1.005	1.343×10^{-2}	0.967	0.837
3.047×10^{-5}	(11)	2.186	1.004	8.683×10^{-3}	0.945	0.698
3.047×10^{-5}	(40)	2.245	1.003	1.426×10^{-2}	0.966	0.781
6.084×10^{-5}	(10)	0.881	1.003	1.328×10^{-2}	0.989	0.918
6.084×10^{-5}	(20)	1.416	1.002	1.699×10^{-2}	1.003	0.883
6.084×10^{-5}	(01)	1.688	1.003	1.288×10^{-2}	0.976	0.790
6.084×10^{-5}	(30)	1.865	1.001	2.010×10^{-2}	0.964	0.791
6.084×10^{-5}	(11)	2.187	1.003	1.309×10^{-2}	0.980	0.654
6.084×10^{-5}	(40)	2.246	1.001	2.106×10^{-2}	0.998	0.747
1.521×10^{-4}	(10)	0.877	0.999	2.127×10^{-2}	1.019	0.907
1.521×10^{-4}	(20)	1.410	0.999	2.827×10^{-2}	1.020	0.838
1.521×10^{-3}	(01)	1.686	1.000	2.212×10^{-2}	0.998	0.727
1.524×10^{-4}	(30)	1.858	0.999	3.287×10^{-2}	1.032	0.765
1.524×10^{-4}	(11)	2.186	1.001	2.419×10^{-2}	1.002	0.560
1.524×10^{-4}	(40)	2.239	1.000	3.694×10^{-2}	1.033	0.674
3.153×10^{-4}	(10)	0.869	0.999	3.099×10^{-2}	1.057	0.896
3.141×10^{-4}	(20)	1.400	1.000	4.292×10^{-2}	1.041	0.794
3.136×10^{-4}	(01)	1.681	1.000	3.432×10^{-2}	1.033	0.672
3.136×10^{-4}	(30)	1.849	0.999	5.104×10^{-2}	1.060	0.706
3.136×10^{-4}	(11)	2.182	1.001	3.892×10^{-2}	1.066	0.499
3.135×10^{-4}	(40)	2.230	1.000	5.851×10^{-2}	1.076	0.609
7.038×10^{-4}	(10)	0.851	1.004	5.105×10^{-2}	1.028	0.812
6.963×10^{-4}	(20)	1.378	1.004	6.985×10^{-2}	1.061	0.726
6.963×10^{-4}	(01)	1.665	1.002	5.969×10^{-2}	1.035	0.576
6.938×10^{-4}	(30)	1.824	1.004	8.837×10^{-2}	1.058	0.606
7.038×10^{-4}	(11)	2.166	1.004	7.462×10^{-2}	1.052	0.390
6.974×10^{-4}	(40)	2.205	1.004	1.066×10^{-1}	1.068	0.497
1.479×10^{-3}	(10)	0.830	1.007	8.293×10^{-2}	1.004	0.725
1.479×10^{-3}	(20)	1.352	1.006	1.102×10^{-1}	1.122	0.671
1.484×10^{-3}	(01)	1.642	1.007	1.065×10^{-1}	1.020	0.471
1.484×10^{-3}	(30)	1.788	1.010	1.458×10^{-1}	1.122	0.537
1.484×10^{-3}	(11)	2.142	1.009	1.321×10^{-1}	1.108	0.320
2.960×10^{-3}	(20)	1.320	1.008	1.985×10^{-1}	1.028	0.527
2.960×10^{-3}	(01)	1.615	1.011	1.809×10^{-1}	1.036	0.392
2.960×10^{-3}	(11)	2.114	1.014	2.473×10^{-1}	1.081	0.241

both HPLC grade water and silicone oil (Tables II and III). Special care is taken in the water experiments to follow closely the experimental protocols of HM, including prior soaking of the container with the same cleaner (Micro-90, International Products Corp.), enclosing the experiment in a protective dust cover, and vacuuming the interface with a water-driven venturi pump. Measurements of damping in water are recorded as rapidly as possible after aspirating the interface—typically within ~ 3 min. Despite these precautions, we find the measured damping rate is effectively reproducible only by the tedious process of refilling and aspirating the interface prior to each run, repeated measurement after aspiration typically yielded noticeably larger damping rates. (HM report reproducible measurement of δ_e over a 3 h period.) Under these conditions, we find δ_e and δ_i agree within 4.6% for the (10), (20), and (30) modes (Table II), in accord with HM.^{5,6} We also find δ_e exceeds δ_i for the (0,1) mode; however, δ_e is $\sim 12\%$ larger in our experiments vs

26% larger in HM.⁵ In our case, the increase of δ_e with time as the interface “aged” suggests the experiments with water are not completely free from interfacial contamination due to surface active agents. By contrast, aspiration and special cleaning procedures are not used for the experiments with silicone oil, whose low surface tension leads to an interface that is highly insusceptible to contamination. We find δ_e and δ_i for silicone oil in the same container for values of C similar to the water experiments agree to better than 5.4% for all modes, including (01) (Table III). No aging effects are observed with silicone oil; δ_e is reproducible over a several hour period, provided the container is refilled to replace oil lost by evaporation. The silicone oil and water runs differ substantially in the value of B (Tables II and III); however, this difference translates into a relatively small difference in δ_i ($\sim 5\%$), when both fluids are at the same value of ν . Thus, we believe these results, as a whole, suggest interfacial contamination in the HPLC water experiments by HM and us may account for the discrepancy with theory for the (01) mode.

Damping rates from theory and experiment typically agree to better than 7% when $C < 10^{-3}$ with silicone oils for both the $\Gamma = 0.725$ and $\Gamma = 4.33$ containers (Tables III and IV). The agreement remains quite good even as C increases such that the higher order bulk damping contribution $a_2 C$ becomes more than four times larger than the leading order Stokes layer contribution $a_1 C^{1/2}$ [e.g., the (01) mode at $C = 7.591 \times 10^{-4}$ in Table III]. It is worth noting that predictions for the $\Gamma = 0.725$ container well-represent the deep-container limit; δ_i is virtually unchanged by taking $\Gamma \rightarrow 0$ for all modes at all values of C studied here. By contrast, the $\Gamma = 4.33$ container better represents the shallow-container regime $\Gamma \gg 1$ where the requirement that the thickness of the Stokes layers be small compared to $1/\Gamma$ ensures that the bulk contribution $a_2 C$ is small for the lowest frequency modes.⁵ Thus, for a given value of C , the bulk contribution is typically significantly more important for describing the measured damping at $\Gamma = 0.725$ than for $\Gamma = 4.33$. For both aspect ratios at fixed C , the bulk damping becomes more important as ω increases; physically, the amplitude of surface wave modes decay spatially as an exponential function of the wave number moving away from the free surface toward the bottom boundary. Thus, since the wave number increases with increasing ω , the Stokes layer dissipation at the container’s bottom quickly becomes negligible and the bulk damping dominates.

For $C > 10^{-3}$ with both aspect ratios, δ_i and δ_e differ by as much as 20% (Tables III and IV). The asymptotic predictions of δ_i should be less accurate with increasing C , requiring higher order terms in Eq. (1), which would typically cause δ_i to increase. However, we find δ_i at $O(C)$ already exceeds δ_e by 8%–20% for 12 out of 16 measurements with $C > 10^{-3}$. Very recently, a similar discrepancy is reported when comparing δ_i from Eq. (1) with an “exact” semianalytic calculation valid for arbitrary values of C .⁷ In particular, for the (01) mode at $C = 2 \times 10^{-3}$, $\Gamma = 0.725$, and $B = 103.2$, δ_i is 15% larger than the damping rate from the exact calculation;⁷ this compares well with our finding that δ_i is 13.5% larger than δ_e for the (01) mode at $C = 1.738$

$\times 10^{-3}$ at the same aspect ratio in silicone oil (Table III). The contribution of systematic experimental error to these discrepancies cannot be ruled out; measurement of δ_e is more difficult at higher damping since the range in time where the log of the amplitude exhibits a well-defined slope [Fig. 2(c)] becomes substantially smaller.

In summary, our results demonstrate that viscous dissipation in both the Stokes layers and the bulk must be included to predict quantitatively decay rate measurements of low frequency Faraday modes over a wide range of C in right circular cylinders. Similar good agreement is expected for other container shapes (e.g., rectangular), but this conjecture remains unverified. The behavior of higher frequency modes also remains unexplored; in this regime, damping at the free surface is expected to become more important and can play an important role in pattern formation.⁸

ACKNOWLEDGMENTS

The authors would like to thank Edgar Knobloch for bringing this problem to our attention. We are particularly grateful to Carlos Martel for his invaluable assistance in the computation of the predicted damping rates and frequencies. The authors have also benefitted from fruitful discussions with Edgar Knobloch, Carlos Martel and Jose Vega. This research has been supported by the NASA Office of Life and Microgravity Sciences, Grant No. NAG3-2006.

- ¹J. C. Scott, "The historical development of wave-calming using oil," Fluid Mechanics Research Institute, University of Essex, Report No. 81 (1977).
- ²T. B. Benjamin and F. Ursell, "The stability of the plane surface of a liquid in vertical periodic motion," Proc. R. Soc. London, Ser. A **225**, 505 (1954).
- ³J. W. Miles and D. M. Henderson, "Surface-wave damping in a circular cylinder with a fixed contact line," J. Fluid Mech. **275**, 285 (1994).
- ⁴J. Graham-Eagle, "A new method for calculating eigenvalues with applications to gravity-capillary waves with edge constraints," Math. Proc. Cambridge Philos. Soc. **94**, 553 (1983).
- ⁵C. Martel, J. A. Nicolás, and J. M. Vega, "Surface-wave damping in a brimful circular cylinder," J. Fluid Mech. **360**, 213 (1998).
- ⁶D. M. Henderson and J. W. Miles, "A note on interior vs boundary-layer damping of surface waves in a circular cylinder," J. Fluid Mech. **364**, 319 (1998).
- ⁷J. A. Nicolás and J. W. Miles, "A note on damping of capillary-gravity waves in a brimful circular cylinder, J. Fluid Mech. (to be published).
- ⁸P. Chen and J. Viñals, "Pattern selection in Faraday waves," Phys. Rev. Lett. **79**, 2670 (1997).
- ⁹A. Kudrolli and J. P. Gollub, "Patterns and spatiotemporal chaos in parametrically forced surface waves: a systematic survey at large aspect ratio," Physica D **97**, 133 (1997).
- ¹⁰J. A. Nicolás and J. M. Vega, "Weakly nonlinear oscillations of nearly inviscid axisymmetric liquid bridges," J. Fluid Mech. **328**, 95 (1996).
- ¹¹N. R. Pallas and Y. Harrison, "An automated drop shape apparatus and the surface tension of pure water," Colloids Surface **43**, 169 (1990).
- ¹²*CRC Handbook of Chemistry and Physics* (CRC, Boca Raton, 1984).
- ¹³H. Gasquet and A. J. Wooten, "Variable-frequency complex demodulation technique for extracting amplitude and phase information," Rev. Sci. Instrum. **68**, 1111 (1997).
- ¹⁴F. Ursell, "Edge waves on a sloping beach," Proc. R. Soc. London, Ser. A **214**, 79 (1952).